THE JOURNAL OF BIOLOGICAL CHEMISTRY VOL. 283, NO. 7, pp. 4261–4271, February 15, 2008

Staphylococcus aureus DsbA Does Not Have a Destabilizing Disulfide

A NEW PARADIGM FOR BACTERIAL OXIDATIVE FOLDING[*] [S]

Received for publication, September 19, 2007, and in revised form, November 14, 2007 Published, JBC Papers in Press, December 12, 2007, DOI 10.1074/jbc.M707838200

Begoña Heras[‡1], Mareike Kurz[‡], Russell Jarrott[‡], Stephen R. Shouldice[‡], Patrick Frei[§], Gautier Robin[‡], Maša Čemažar[‡], Linda Thöny-Meyer[¶], Rudi Glockshuber[§], and Jennifer L. Martin[‡2]

From the [‡]Institute for Molecular Bioscience, University of Queensland, Brisbane QLD 4072, Australia, the [§]Institute of Molecular Biology and Biophysics, ETH Zürich CH-8093 Zürich, Switzerland, and the [¶]Laboratory for Biomaterials, EMPA, Lerchenfeldstrasse 5, CH-9014 St. Gallen, Switzerland

In Gram-negative bacteria, the introduction of disulfide bonds into folding proteins occurs in the periplasm and is catalyzed by donation of an energetically unstable disulfide from DsbA, which is subsequently re-oxidized through interaction with DsbB. Gram-positive bacteria lack a classic periplasm but nonetheless encode Dsb-like proteins. *Staphylococcus aureus* encodes just one Dsb protein, a DsbA, and no DsbB. Here we report the crystal structure of *S. aureus* DsbA (SaDsbA), which incorporates a thioredoxin fold with an inserted helical domain, like its *Escherichia coli* counterpart EcDsbA, but it lacks the characteristic hydrophobic patch and has a truncated binding groove near the active site. These findings suggest that SaDsbA has a different substrate specificity than EcDsbA. Thermodynamic studies indicate that the oxidized and reduced forms of SaDsbA are energetically equivalent, in contrast to the energetically unstable disulfide form of EcDsbA. Further, the partial complementation of EcDsbA by SaDsbA is independent of EcDsbB and biochemical assays show that SaDsbA does not interact with EcDsbB. The identical stabilities of oxidized and reduced SaDsbA may facilitate direct re-oxidation of the protein by extracellular oxidants, without the need for DsbB.

The formation of native disulfide bonds through air oxidation of cysteine pairs is a slow reaction and organisms ranging from bacteria to humans encode enzymatic systems to catalyze the process. In eukaryotes, oxidative folding in the endoplasmic reticulum is primarily catalyzed by protein-disulfide isomerases that are reoxidized by Ero1p/Erv2p proteins (reviewed in Ref. 1). In *Escherichia coli*, dithiol oxidation takes place in the periplasm through the action of the Dsb[3] (Disulfide bond) family of proteins. Dsb proteins form two distinct pathways, the DsbA-DsbB (oxidative) pathway that introduces disulfides indiscriminately, and the DsbC/DsbG-DsbD (isomerization) pathway that shuffles incorrect disulfides (2, 3).

Probably the best-studied Dsb protein is EcDsbA, the primary disulfide catalyst in *E. coli* (reviewed in Refs. 2, 4). This promiscuously oxidizing protein is a 21-kDa monomer containing a CPHC active site in a thioredoxin (TRX) fold with an inserted helical domain of ~80 residues. Upon catalyzing disulfide bond formation in substrate proteins, reduced EcDsbA relies on EcDsbB, a quinone reductase, to recover its catalytically active, and higher energy, oxidized form (5). Orthologs of DsbA are encoded in many Gram-negative bacteria and have been shown to play an essential role in the biogenesis of virulence factors and toxins in pathogenic organisms (6–12).

Although Gram-positive organisms do not have a conventional periplasm, they contain a compartment confined between the plasma membrane and the outer cell wall (13, 14) and genomic analysis indicates that they do encode cell surface anchored Dsb-like proteins (15). Functional orthologs of Dsb proteins in Gram-positive organisms include *Bacillus brevis* Bdb (a DsbA ortholog) (16), *Bacillus subtilis* BdbB and BdbC (orthologs of DsbB), *B. subtilis* BdbD (a DsbA ortholog) (17–21) and *Mycobacterium tuberculosis* DsbE (structurally a homolog of DsbE, but functionally an oxidant like DsbA) (22). Moreover, functional virulence factors produced by Gram-positive bacteria, such as the human pathogen *Staphylococcus aureus*, contain disulfide bonds that are introduced during folding (23–25).

S. aureus and other pathogens such as *Listeria monocytogenes* and *Enterococcus faecalis* belong to a subgroup of Gram-positive bacteria that encode only a homolog of DsbA and lack other Dsb proteins (15). *S. aureus* DsbA (SaDsbA) (26), is a

* This work was supported in part by an Australian National Health and Medical Research Council (NHMRC) Senior Research Fellowship (to J. L. M.), Australian Research Council grants (to J. L. M. and to B. H.), a University of Queensland Early Career Researcher Grant (to B. H.), an International Postgraduate Research Scholarship (IPRS) (to M. K.), a University of Queensland Postdoctoral Fellowship (to S. R. S.), an ARC Postdoctoral fellowship (to M. C.), and the Schweizerische Nationalfonds within the framework of the NCCR Structural Biology Program (to R. G. and P. F.). The costs of publication of this article were defrayed in part by the payment of page charges. This article must therefore be hereby marked "*advertisement*" in accordance with 18 U.S.C. Section 1734 solely to indicate this fact.

The atomic coordinates and structure factors (code 3BCI, 3BD2, and 3BCK) have been deposited in the Protein Data Bank, Research Collaboratory for Structural Bioinformatics, Rutgers University, New Brunswick, NJ (http://www.rcsb.org/).

[S] The on-line version of this article (available at http://www.jbc.org) contains supplemental Fig. S1.

[1] To whom correspondence may be addressed: Queensland Bioscience Precinct, Bldg. 80 Carmody Rd, University of Queensland QLD 4072, Australia. Tel.: 61-7-33462020; Fax: 61-7-33462101; E-mail: bheras@imb.uq.edu.au.

[2] To whom correspondence may be addressed: Queensland Bioscience Precinct, Bldg 80 Carmody Rd, University of Queensland, QLD 4072, Australia. Tel.: 61-7-33462016; Fax: 61-7-33462101; E-mail: j.martin@imb.uq.edu.au.

[3] The abbreviations used are: Dsb, disulfide bond family; DTT, dithiothreitol; r.m.s.d., root mean square deviation; SaDsbA, *S. aureus DsbA;* EcDsbA, *E. coli* DsbA; TRX, thioredoxin; GdmCl, guanidine hydrochloride, Q1, ubiquinone-1; RNase A, ribonuclease A; IAM, iodoacetamide.

23-kDa lipoprotein that has low sequence homology with EcDsbA (15% amino acid identity) and lacks residues thought to be important for DsbA function in Gram-negative organisms, including a His in the CXHC active site motif and a Val preceding the *cis*-Pro (V*c*P) active site motif. Instead, SaDsbA has residues in these two motifs that are more typical of the Gram-negative disulfide isomerases DsbC and DsbG (CXYC, T*c*P). Despite these differences, the soluble form of SaDsbA can partially complement EcDsbA in a Δ*dsbA* background (26). Moreover, SaDsbA can replace each of the disulfide oxidoreductases of *B. subtilis* (BdbA-D) that catalyze the oxidative folding of specific extracytoplasmic proteins (15). Despite some ability to complement DsbA function in these organisms, its low sequence identity suggests that SaDsbA has a different purpose, most likely to act on different, as yet unidentified target protein(s). Notably, the activity of SaDsbA in both *E. coli* and *B. subtilis* does not depend on re-oxidation by a DsbB-like disulfide oxidoreductase (15, 26). Indeed, *S. aureus* does not encode a DsbB nor any other Dsb-like proteins.

To investigate how SaDsbA catalyzes disulfide bond formation without the need for a partner disulfide shuttle protein, we determined the crystal structure of SaDsbA, representing the first such Gram-positive DsbA structure, and analyzed its biochemical and functional properties. Our findings show that the physicochemical basis for oxidative folding in *S. aureus* is very different to that underpinning Gram-negative oxidative folding.

EXPERIMENTAL PROCEDURES

Cloning, Expression, and Protein Production—Native SaDsbA was prepared as previously described (27). Briefly, SaDsbA containing a C-terminal hexahistidine tag was purified using cobalt-chelate chromatography, followed by gel filtration and ion-exchange chromatography (Superdex S-200 and Mono S 5/50, GL column, GE Healthcare). SaDsbA was oxidized before crystallization by addition of 1.7 mM copper(II) 1,10-phenanthroline.

Selenomethionine (SeMet)-labeled SaDsbA was expressed from BL21(DE3) pLysS strain in minimal medium containing SeMet (L/D mixture) using methods similar to those described previously (28). SaDsbA variants were generated using a Stratagene Quikchange kit (Stratagene, CA) and verified by DNA sequencing. SeMet SaDsbA and all SaDsbA variants were expressed and purified following the same procedures described for native SaDsbA.

Crystallization and Diffraction Data Measurement—Native and selenomethionine (SeMet)-labeled SaDsbA crystals were obtained from 28–30% PEG 3350. MAD data were collected at the 8.3.1 beam line at the Advance Light Source (ALS) in Berkeley. Diffraction data were integrated and scaled with HKL2000 (29). Native, SaDsbA E96Q, and SaDsbA T153V data were measured using a Rigaku FR-E copper rotating anode generator operating at 45 kV, 45 mA with Osmic Confocal Max-Flu™ optics (either HiRes^2 or Maxscreen). Reflections were measured with an R-AXIS IV^{++} imaging plate area detector (Rigaku Americas). A Cryo Industries CryoCool LN2 was used for cooling the crystals during data measurement. Data were processed using Crystal Clear (Rigaku).

Structure Determination—The structure of SaDsbA was solved by MAD phasing of the SaDsbA-SeMet derivative. The two possible selenium positions were located in the asymmetric unit with the program SOLVE/RESOLVE (30). The resulting phases were used in the program ARP/WARP for automated building of the protein structure (31). The structure was completed by manual building using the programs O (32) and Coot (33).

Refinement was performed using maximum likelihood in CNS (34) on the native 1.81-Å resolution dataset. The final model corresponds to residues 14–177 of the deduced mature protein. Some surface residues with weak electron density were modeled with reduced occupancies for the side chain atoms (Glu^{104}, Lys^{133}, Glu^{170}, Lys^{174}).

The structure of SaDsbA variants were solved by difference Fourier or molecular replacement (Phaser (35)) methods by using the structure of native SaDsbA. Superposition of molecules was carried out using the LSQ options from the programs O (32) and Coot (33).

Molecular figures were generated using MolScript (36) and PyMOL (37) and figures of the electrostatic potential were generated using GRASP (38).

GdmCl-induced Unfolding Equilibria—For the chemical unfolding experiments, proteins were diluted to 1.5 μM in 20 mM Hepes-NaOH, 170 mM NaCl, 0.1 mM EDTA, pH 7.0 buffer containing increasing concentrations of GdmCl and incubated at room temperature for 24 h. The reduced proteins were unfolded under identical conditions but in the presence of 0.75 mM DTT. For the refolding experiments oxidized and reduced protein stock solutions (37.5 μM) were unfolded in 20 mM Hepes-NaOH, 170 mM NaCl, 0.1 mM EDTA (pH 7.0), 6 M GdmCl, (containing 20 mM DTT in the case of reduced proteins) for 16 h at room temperature. Then 20 μl of these solutions were mixed with 480 μl of buffers containing different concentrations of GdmCl and incubated for 24 h at room temperature. Transitions were measured fluorimetrically by the change in the fluorescence at 330 nm using an excitation wavelength of 280 nm. Data were evaluated according to the two-state model of folding using a six parameter fit (39).

Thermal Unfolding—Temperature-induced unfolding curves of native SaDsbA and variants were monitored by the change in the far-UV circular dichroism (CD) signal. Far-UV CD spectra (from 250 to 190 nm) of 10 μM protein solutions were recorded at 25 and 95 °C on a Jasco J-715 spectropolarimeter. The wavelength with the largest change in signal was determined from the differential spectrum at 25 and 95 °C. Thermal unfolding was monitored at 223 nm from 25–90 °C with a heating-rate of 1 °C/min. All measurements were carried out in 100 mM phosphate buffer, 1 mM EDTA pH 7.0 (in the presence of 0.75 mM DTT for reduced proteins) using a 1-mm quartz cuvette. Transitions were normalized by assuming a linear dependence of the spectroscopic signal of the native and unfolded states on temperature.

Determination of the Equilibrium Constants with Glutathione—The redox equilibrium of SaDsbA and SaDsbA variants was determined as described previously (40). Briefly, 1.5 μM protein was incubated for 16 h at 25 °C in 100 mM sodium phosphate, 0.1 mM EDTA (pH 7.0) containing 1 mM GSSG

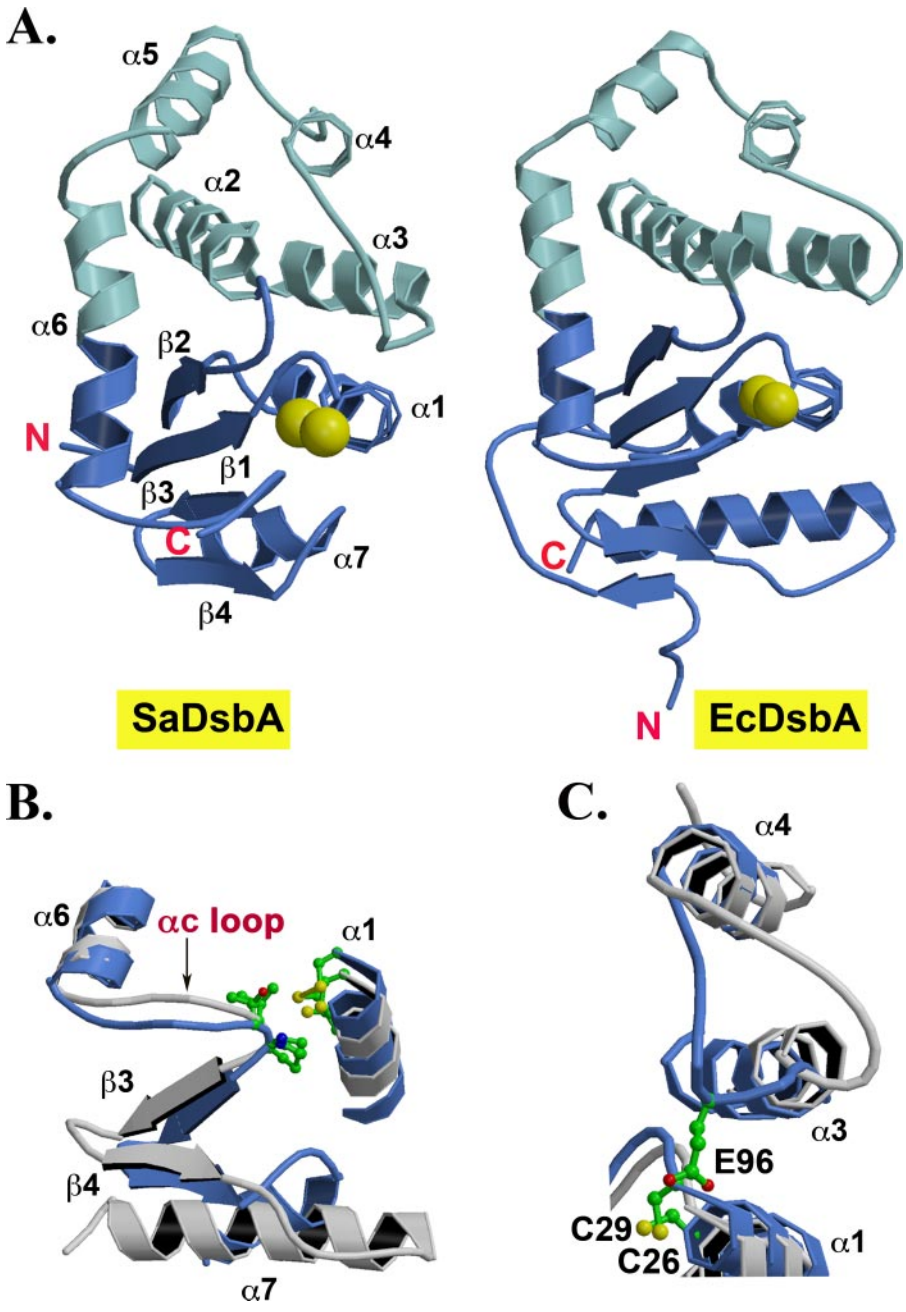

FIGURE 1. **Structure of SaDsbA.** *A*, *ribbon representations* of SaDsbA and EcDsbA crystal structures. Both structures incorporate a TRX fold (*dark blue*) with a helical insertion (*light blue*). The active site disulfide is shown in space-filling representation (*yellow*) and secondary structural features of SaDsbA are labeled. *B*, superposition of SaDsbA (*blue*) and EcDsbA (*gray*), showing the structural differences at the $\beta3\beta4\alpha7$ motif, which forms one edge of the proposed peptide-binding groove in EcDsbA (48), and at the αc loop (linking $\alpha6$ with $\beta3$). Residues in the active sites of both proteins, including the catalytic cysteines (*E. coli* Cys^{30}, Cys^{33}, and *S. aureus* Cys^{26}, Cys^{29}), and *cis*-proline loop residues (*E. coli* Val^{150}, Pro^{151}, and *S. aureus* Thr^{153}, Pro^{154}) are shown in *ball-and-stick representation*. *C*, superposition of SaDsbA (*blue*) and EcDsbA (*gray*), showing the loop connecting helices $\alpha3$ and $\alpha4$. In SaDsbA the loop has an additional residue and is located much nearer to the ^{26}CPYC^{29} redox catalytic site, positioning an acidic residue (*E96*) near the nucleophilic cysteine *C26*.

and increasing concentrations of GSH. The redox state of the SaDsbA was followed by fluorescence emission at 335 nm. The equilibrium constant K_{eq} and redox potential were determined according to standard thermodynamic equations (41).

Determination of pK_a Values—The pH-dependent ionization of the nucleophilic cysteine thiol was followed by the specific absorbance of the thiolate anion at 240 nm (42). As a reference, the pH-dependent absorbance for the oxidized form of the protein was monitored. All measurements were carried out at 25 °C in pK_a buffer consisting of 10 mM K_2HPO_4, 10 mM boric acid, 10 mM sodium succinate, 1 mM EDTA, and 200 mM KCl, pH 7.5 and an average initial protein concentration of 20 μM. The oxidized and reduced protein samples were prepared by incubating the proteins with 1.7 mM copper(II)[1,10-phenanthroline] and 10 mM DTT, respectively. The oxidizing and reducing agents were eliminated by gel filtration using a PD10 column equilibrated in pK_a buffer. The pH of the protein solution was lowered to 2.2 stepwise by the addition of aliquots of 0.2 M HCl. The absorbance at 240 and 280 nm was recorded on a Cary 50BIO UV-visible spectrophotometer and corrected for the volume increase. The pH dependence of the thiolate-specific absorbance signal ($S = (A_{240}/A_{280})_{reduced}/(A_{240}/A_{280})_{oxidized}$) was fitted according to the Henderson-Hasselbalch equation.

Insulin Reduction Assay—The ability of SaDsbA and SaDsbA variants to catalyze insulin reduction in the presence of DTT was determined as previously described (43). Briefly, reaction mixtures were prepared in cuvettes containing 131 μM insulin, and various concentrations of oxidized protein catalyst (5–10 μM) in 0.1 M phosphate buffer, pH 7.0, 2 mM EDTA. Reactions were started by adding DTT to a final concentration of 0.35 mM. After thorough mixing, the optical density at 650 nm was recorded every 30 s. The non-catalyzed reduction of insulin by DTT was monitored in a control reaction without catalyst.

Ubiquinone Reduction Assay—To determine the EcDsbB-catalyzed oxidation of SaDsbA by ubiquinone Q1 *in vitro*, 15 μM reduced SaDsbA in 50 mM sodium phosphate, 300 mM NaCl, 0.1% (w/v) *n*-dodecyl-D-maltoside, pH 6.0, were incubated at 30 °C with 15 μM ubiquinone-1 (Q1; Sigma) (44). The reaction was started by the addition of DsbB to a final concentration of 0.1 μM and the reduction of Q1 was monitored through the decrease in absorbance at 275 nm. EcDsbA was used as a positive control.

TABLE 1
Data collection and refinement statistics

	SaDsbA MAD (SeMet)			SaDsbA Native	SaDsbA E96Q	SaDsbA T153V
Data collection						
Wavelength (Å)	0.9796	0.9797	0.95373	1.54	1.54	1.54
Resolution range (Å)	50–1.99 (2.06–1.99)	50–1.99 (2.06–1.99)	50–2.10 (2.18–2.10)	37.1–1.81 (1.86–1.81)	50.0–1.81 (1.87–1.81)	62.4–1.95 (2.02–1.95)
a, *b*, *c*, (Å, Å, Å)		72.6, 72.6, 92.6		72.10, 72.10, 92.10	72.42, 72.42, 92.68	72.09, 72.09, 92.57
Space group	$P6_5$	$P6_5$	$P6_5$	$P6_5$	$P6_5$	$P6_5$
Observed reflections	156,671	156,464	134,695	236,650	108,649	97,543
Unique reflections	19,033[a]	19,036[a]	16,161[a]	24,921	24,249	19,271
R_{merge}[b,c]	0.08 (0.32)	0.07 (0.33)	0.07 (0.21)	0.05 (0.38)	0.04 (0.26)	0.07 (0.52)
Completeness (%)[c]	100 (99.7)	99.9 (99.5)	100 (100)	99.1 (91.6)	96.0 (84.8)	96.8 (92.0)
$<I>/<\sigma(I)>$[c]	22.1 (3.9)	24.0 (3.9)	28.1 (6.7)	21.9 (3.3)	33.5 (4.1)	9.3 (2.1)
Phasing statistics						
Resolution (Å)	50-2.1					
No. of selenium sites	2					
Mean figure of merit	0.34					
Refinement statistics						
Number of reflections in working set/test set				24,569/2,432	23,741/3,060	19,156/2,880
R_{fac}[d]/R_{free}[e] (%)[c]				19.8/21.9 (37.0/39.5)	24.2/25.5 (38.5/38.8)	22.2/25.1 (43.7/41.2)
Number of waters				231	225	155
R.m.s.d from ideal geometry						
Bonds (Å)				0.006	0.006	0.008
Angles (°)				1.2	1.2	1.4
Ramachandran plot						
Most favoured/additionally allowed regions (%)				92.8/7.2	92.8/7.2	90.8/9.2
Average B factor (Å^2)				35.5	32.0	44.9

[a] Friedel pairs kept separate.
[b] $R_{merge} = \Sigma|I - <I>|/\Sigma<I>$ where I is the intensity of individual reflections.
[c] Values in parentheses refer to the highest resolution shell.
[d] $R_{fac} = \Sigma_h|F_o - F_c|/\Sigma_h|F_o|$, where F_o and F_c are the observed and calculated structure-factor amplitudes for each reflection "h".
[e] R_{free} was calculated with 10% of the diffraction data selected randomly and excluded from refinement.

Refolding of Scrambled RNase A—The *in vitro* assay of refolding of scrambled RNase was used to monitor the isomerase activity of SaDsbA (45). scRNase was prepared from reduced denatured RNase by incubating the enzyme (0.5 mg/ml) in 50 mM Tris-HCl, pH 8.5 and 6 M GdmCl for at least 3 days at room temperature and in the dark. After acidifying the solution as previously described, the fully oxidized state of RNase A was confirmed by Ellman's assay. Reshuffling of scRNase (40 μM) was carried out by incubation in 100 mM phosphoric acid-NaOH, pH 7.0, 1 mM EDTA, with 10 μM oxidized DsbC or oxidized SaDsbA. The reactions were started by addition of DTT to a final concentration of 10 μM. As positive and negative controls we carried out two additional reactions using folded RNase and scRNase, respectively, and without any Dsb protein. The assay was performed at 25 °C and at several time points samples were withdrawn and assayed for RNase A activity by monitoring cCMP hydrolysis.

Coordinates and structure factors for SaDsbA, SaDsbA E96Q, and SaDsbA T153V have been deposited in the Protein Data Bank (PDB ID codes 3BCI, 3BD2, and 3BCK, respectively).

RESULTS

Structure of SaDsbA—The crystal structure of soluble SaDsbA (Fig. 1*A*), the deduced mature protein, was determined by multiwavelength anomalous diffraction methods (46, 47) and refined at 1.81-Å resolution to *R*-factor and *R*-free values of 19.8 and 21.9%, respectively (Table 1). The structure of SaDsbA reveals a fold similar to that of EcDsbA comprising a thioredoxin (TRX) domain and an embedded helical domain (Fig. 1*A*). The classic TRX fold is composed of residues 17–58 forming the $\beta\alpha\beta$ motif and residues 155–181 forming the $\beta\beta\alpha$ motif with the connecting helix formed by residues 142–154. The 82-residue insertion in the TRX fold of SaDsbA (residues 59–141) forms an antiparallel three-helical bundle (α2-α4), an additional helix (α5) and an extension to helix α6. As in all redox-active TRX-like proteins, the TRX fold of SaDsbA includes a C*XX*C motif (Cys^{26}-Pro^{27}-Tyr^{28}-Cys^{29}) located at the N terminus of the first helix in the TRX fold (Fig. 1*A*).

Comparison with E. coli DsbA—The overall fold of SaDsbA resembles that of EcDsbA; the Cα atoms of 110 residues can be superimposed with an r.m.s.d. of 1.9 Å, and the sequence identity is 15%. Despite the structural similarity, the two proteins have critical differences in regions surrounding the catalytic C*XX*C motif that could impact on substrate specificity and activity. These regions include the β3β4α7 ($\beta\beta\alpha$) motif of the TRX fold (Fig. 1*B*) and loops connecting helices in the inserted helical domain, primarily the loop between α3 and α4 (Fig. 1*C*). The β3β4α7 motif at the C-terminal end of the polypeptide chain produces a dramatic difference between SaDsbA and EcDsbA (Fig. 1*B*). This region forms one edge of a hydrophobic peptide-binding groove in EcDsbA (48) that binds to DsbB (49) and is proposed to interact with unfolded protein substrates. In both proteins this region is hydrophobic, however in SaDsbA it is 9 residues shorter, resulting in a shorter loop connecting β4 and α7 and a shorter α7 helix (by two turns) (Fig. 1*B*). Based on sequence alignment, this deletion appears to be conserved in DsbAs from Gram-positive organisms and, to a lesser extent in some Gram-negative DsbA proteins such as TcpG from *Vibrio cholerae* (Fig. 2*A*).

Another notable difference between SaDsbA and EcDsbA occurs in the loop connecting helices α3 and α4. Compared with EcDsbA, this loop has an extra residue in SaDsbA and is oriented toward the C*XX*C active site, positioning the acidic side chain of Glu^{96} near to the nucleophilic Cys^{26} (6.9 Å) (Fig. 1*C*). Sequence alignment shows that acidic residues are highly abundant in this loop in Gram-positive DsbAs but

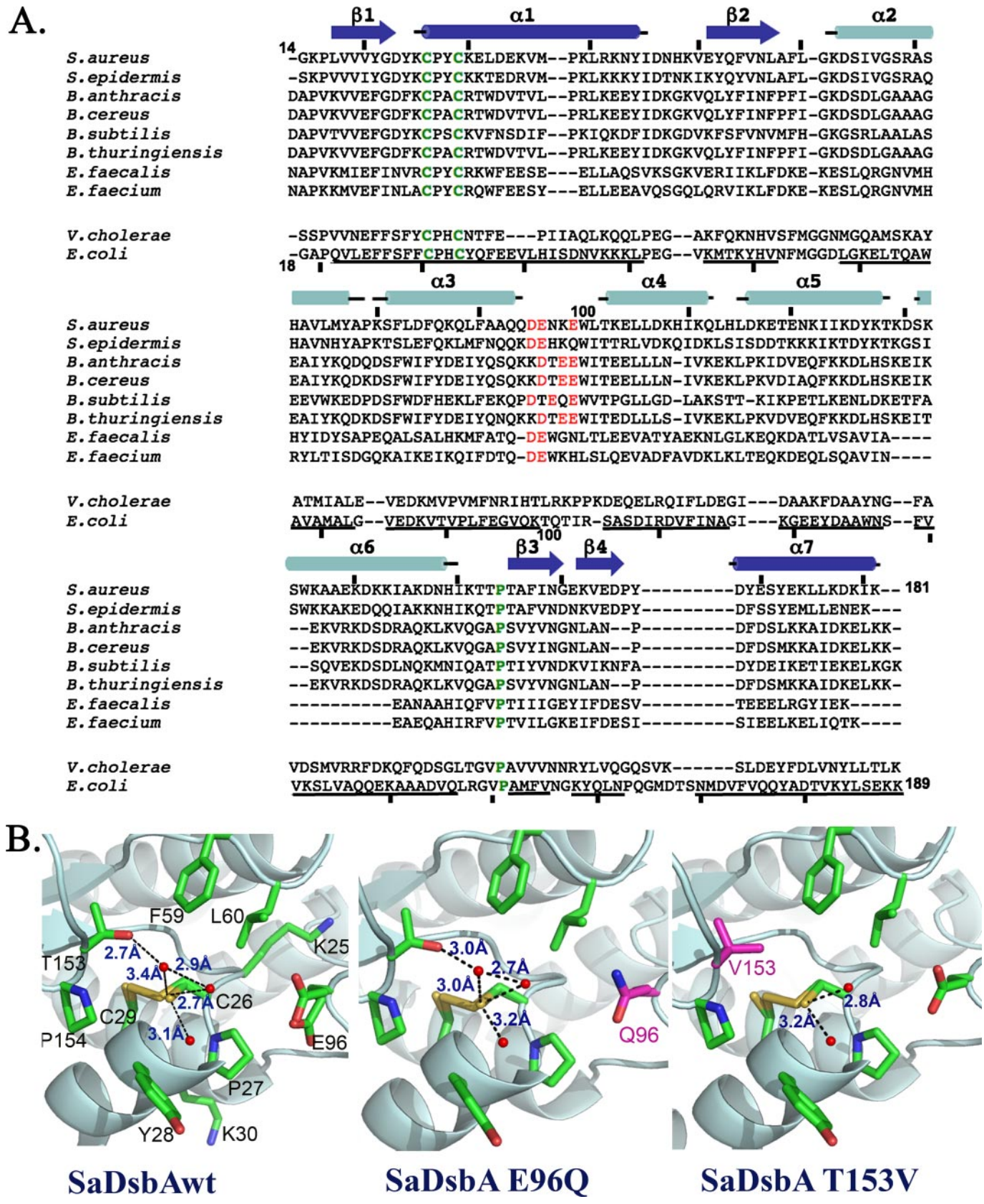

FIGURE 2. *A*, multiple sequence alignment of DsbA homologs from Gram-positive organisms, *V. cholerae* and *E. coli* DsbA. Organisms: *S. aureus*, *S. epidermidis*, *B. anthracis*, *B. cereus*, *B. subtilis*, *B. thuringiensis*, *E. faecalis*, *E. faecium*, *V. cholerae*, and *E. coli*. *Underlined residues* indicate regions of EcDsbA that can be structurally aligned with SaDsbA. (Identical residues are shown in *green*, negatively charged residues in α3-α4 loop are shown in *red*.) *B*, close-up view of the SaDsbAwt, SaDsbA E96Q, and SaDsbA T153V active sites showing the CPYC motif (modeled as a mixture of both redox forms), the residues adjacent to the catalytic motif and the hydrogen bond interactions stabilizing the reduced form. T153V mutation results in the removal of water-mediated hydrogen bonds to the Cys^{26} thiolate.

absent in *E. coli* DsbA (Fig. 2*A*). The proximity of Glu[96] to the redox active site of SaDsbA (Fig. 2*B*) suggests a possible role in substrate specificity or in modulating the redox characteristics.

A *cis*-Pro loop is conserved among redox-active TRX-fold containing proteins and has been shown to be involved in substrate recognition (50–52). SaDsbA contains a Thr preceding the *cis*-Pro residue (T*c*P) a motif that is highly conserved in Gram-negative disulfide isomerases (DsbC and DsbG) but not in Gram-negative oxidases like EcDsbA (which generally have V*c*P). Superposition of SaDsbA and EcDsbA structures reveals a shift in the position of the α*c* loop that precedes the *cis*-Pro loop (Fig. 1*B*). Similar changes in this loop are associated with the different substrate specificities of the disulfide isomerases DsbC and DsbG (53).

Surface Features—EcDsbA has a hydrophobic patch and a peptide-binding groove incorporating a hydrophobic pocket (Fig. 3*A*) that are thought to be important for activity (48). By contrast, the electrostatic surface of SaDsbA shows that it lacks these features. First, the hydrophobic patch adjacent to the active site in EcDsbA is absent in SaDsbA (Fig. 3*A*). Hydrophobic residues that contribute to this patch in EcDsbA (Phe[29] preceding the C*XX*C active site, Phe[63]-Met[64]-Gly[65]-Gly[66] in the loop connecting the TRX and helical domains) are replaced or covered with charged residues in SaDsbA (supplemental Fig. S1). Thus, a basic rather than a hydrophobic residue (Lys[25]) precedes the C*XX*C active site and, although residues of the interdomain loop (Lys[62]–Asp[63]) are mainly hydrophobic, the different conformation of the α3–α4 loop in SaDsbA results in charged residues (Lys[98], Glu[99]) covering this area which flanks the active site. Moreover, the different position of the α3–α4 loop in SaDsbA also results in an acidic protrusion (generated by E96) near the redox active site (Fig. 3*A* and supplemental Fig. S1).

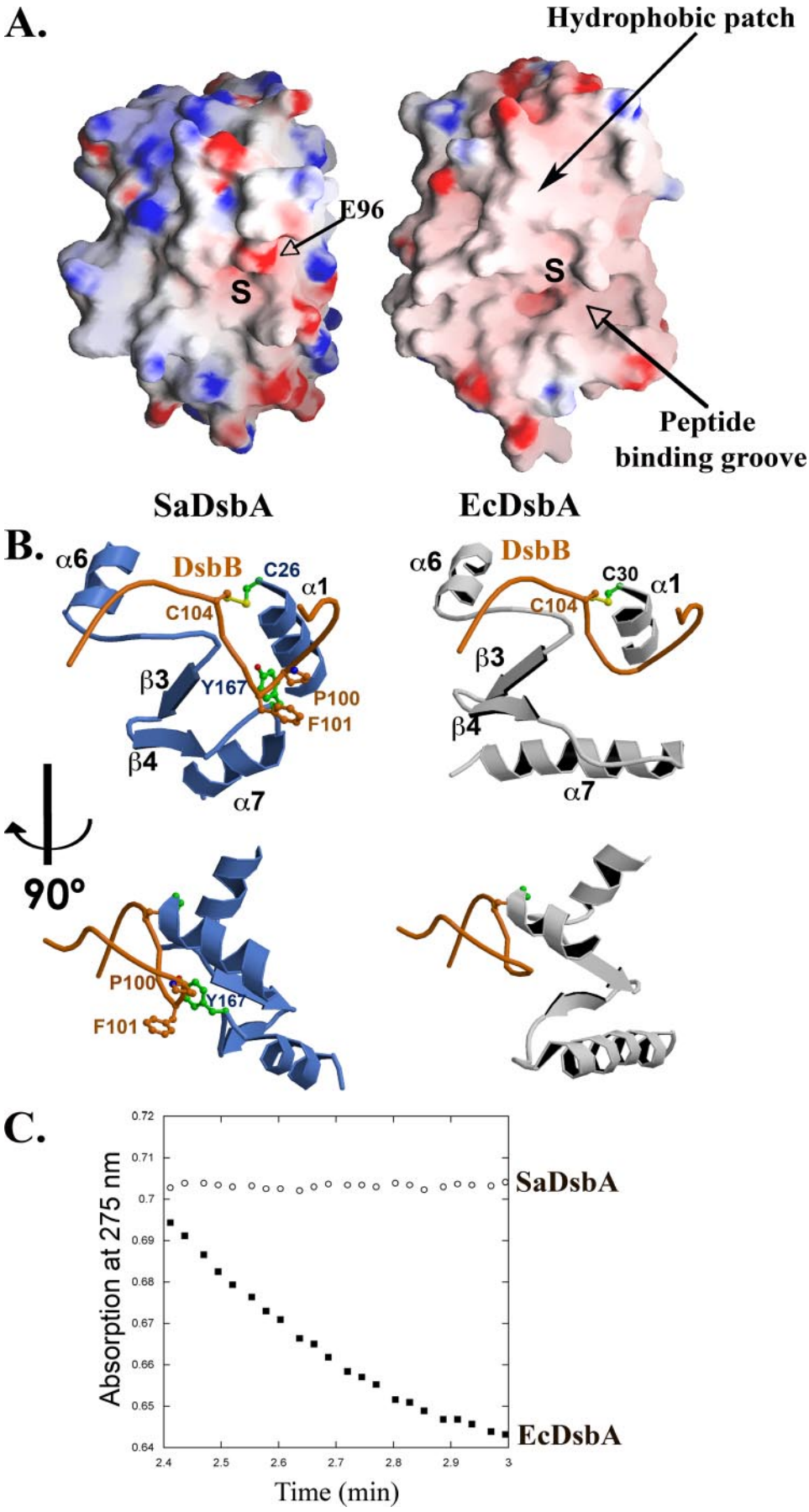

The 9-residue deletion at the C terminus of SaDsbA affects the surface properties in that the peptide binding groove is truncated compared with EcDsbA (Fig. 3*A*). This groove is used by EcDsbA to interact with its partner protein DsbB (49) and has been proposed to be important for substrate binding interactions (54). The altered groove and the lack of a hydrophobic patch in SaDsbA suggest a differing substrate specificity to EcDsbA and indicates that SaDsbA may be unable to interact with DsbB-like quinone oxidoreductases. Indeed, when we modeled the DsbB periplasmic loop of the EcDsbA:DsbB complex (49) into the structure of SaDsbA, steric clashes are predicted as a consequence of the truncated peptide binding groove (Fig. 3*B*). For example, Tyr^{167} in the $\beta4$-$\alpha7$ loop in SaDsbA clashes with residues Pro^{100} and Phe^{101} in DsbB (Fig. 3*B*). Furthermore, when we tested *in vitro* the ability of DsbB to oxidize SaDsbA by monitoring EcDsbB-catalyzed ubiquinone reduction (44), we found that EcDsbB was able to oxidize EcDsbA in a ubiquinone-dependent manner, as expected, but we could not detect SaDsbA oxidation (Fig. 3*C*). These results are in agreement with a novel mechanism of DsbA oxidation in *S. aureus* differing from that performed by DsbB in *E. coli*.

SaDsbA Variants—Two of the most striking sequence and structural differences between SaDsbA and EcDsbA localize to the redox active site; namely, the acidic residue Glu^{96} close to the C*XX*C motif and the T*c*P (rather than V*c*P) in the *cis*-Pro loop. We therefore generated two variants of SaDsbA, E96Q (to remove the acidic residue) and T153V (to generate the same *cis*-Pro sequence as in EcDsbA) for further studies. Their structures were solved showing that the mutations did not affect the overall structure. Thus, the *wt* and variant SaDsbA structures can be superposed with an average r.m.s.d. of 0.14 Å and 0.15 Å for T153V and E96Q, respectively, and the two variants can be superposed with an average r.m.s.d. of 0.16 Å.

SaDsbA Does Not Have a Destabilizing Disulfide—Although most protein disulfides stabilize their protein fold, the catalytic disulfide of EcDsbA is destabilizing (55, 56) This unusual characteristic drives the EcDsbA catalyzed thiol-disulfide exchange reaction in substrate proteins, and is reflected in the highly oxidizing nature of EcDsbA. This characteristic requires that EcDsbA is re-oxidized by DsbB to the more unfavorable, but catalytically active, oxidized form. We determined the thermodynamic stabilities (ΔG_{stab}) of oxidized and reduced SaDsbA and SaDsbA variants with equilibrium unfolding/refolding experiments induced by guanidinium chloride. The transitions were fully reversible for all three SaDsbA proteins (Fig. 4*A*) and the unfolding curves were all highly cooperative and fitted a two state model (57). Surprisingly, the data showed that the oxidized and reduced forms of all three SaDsbA proteins have similar stabilities (Table 2). This was confirmed by temperature-induced unfolding experiments (Fig. 4*B*). For these experiments, EcDsbA was used as a control and the unfolding curves confirmed previous findings that reduced EcDsbA is more stable than oxidized EcDsbA (Table 2). However, oxidized and reduced SaDsbA were found to have similar stabilities (Table 2).

Redox Potential of the Active Site Disulfide—Previous work has shown that SaDsbA ($E'_0 = -131$ mV (26) is not as strong an oxidant as EcDsbA ($E'_0 = -122$ mV (40)). We measured the redox potential for the two SaDsbA variants, using *wt* SaDsbA (26) as a control (Fig. 4*C*). Mutation of the Thr in the *cis*-Pro loop of SaDsbA to Val (T153V, the residue present in EcDsbA), resulted in a redox potential similar to SaDsbA. However, the E96Q mutant yielded a redox potential a little more oxidizing than that of EcDsbA (Fig. 4*C* and Table 2B).

pK_a of the Nucleophilic Cysteine—An important characteristic of thiol-disulfide oxidoreductases is the lowered pK_a of the reactive cysteine, which determines reactivity in thiol-disulfide exchange reactions. Thus, the nucleophilic cysteine of EcDsbA has a pK_a of 3.3, much lower than the typical value for cysteine residues of ~8.5 (42). We measured the pK_a of Cys^{26}, the nucleophilic cysteine of SaDsbA (Fig. 4*D*), and found it to be 3.37, similar to that of EcDsbA. The E96Q variant had a slightly lower pK_a of 3.09. However, the pK_a for the SaDsbA T153V variant was dramatically different with a value of 5.21. To confirm these pK_a values we also measured the pH dependence of the nucleophilic cysteine reactivity with iodoacetamide (IAM) (42). Protein samples were incubated with IAM and after different incubation times the reaction was quenched and reaction products were analyzed by reverse phase HPLC. For *wt* SaDsbA and SaDsbA E96Q the reaction at pH 3.5 was over in less than 2 min, whereas for SaDsbA T153V the reaction took 1 h to complete (data not shown), supporting the finding that it has a higher pK_a.

Disulfide Reductase Activity—Insulin contains two intramolecular disulfide bonds that link the A and B chains. Reduction of these disulfides causes the two chains to dissociate and the insoluble B chain to precipitate. Disulfide reductase activity can thus be assessed by monitoring the increase in turbidity of an insulin solution in the presence and absence of possible reductases. Most TRX-like oxidoreductases, including EcDsbA and EcDsbC, are active in this assay, though EcDsbA has only about 10% the activity of DsbC. We determined the rate of insulin reduction by DTT catalyzed by SaDsbA. Unlike EcDsbA, SaDsbA did not show any activity suggesting that its less hydrophobic surface features do not allow interaction with insulin (Fig. 5*A*). The T153V variant that emulates EcDsbA in the residue preceding the *cis*-Pro at the active site, partially restores reductase activity (Fig. 5*A*). Conversely, the equivalent replacement on EcDsbA (V150T) abolishes EcDsbA insulin reductase activity (data not shown), supporting the

FIGURE 3. *A*, electrostatic surfaces of SaDsbA and EcDsbA. Positive and negative electrostatic potentials are shown in *blue* and *red*, respectively (saturation at 15 kT/e) for each of the proteins. The C*XX*C active site is denoted by *S* for sulfur, and the surface characteristics are labeled. The orientation corresponds to that in Fig. 1, *panel A B*, *right panels*: close up of the *E. coli* DsbA:DsbB complex showing the DsbB periplasmic loop (*orange*) in the EcDsbA hydrophobic groove (*gray*) (PDB code 2hi7) (49). The Cys^{30} (EcDsbA)-Cys^{104} (EcDsbB) disulfide bond is shown in *ball-and-stick representation*. *Left panels*, model of the interaction of the EcDsbB periplasmic loop with SaDsbA showing that binding is impeded by steric clashes between SaDsbA residue Tyr^{167} and EcDsbB residues Pro^{100} and Phe^{101}. *C*, EcDsbB catalyzed reduction of ubiquinone-1 (Q1). Reduced SaDsbA (○) was incubated with ubiquinone-1 and the reaction started by adding DsbB. The reduction of Q1 was monitored by the absorbance decrease at 275 nm. As a positive control the reaction was carried out with EcDsbA (■) in place of SaDsbA.

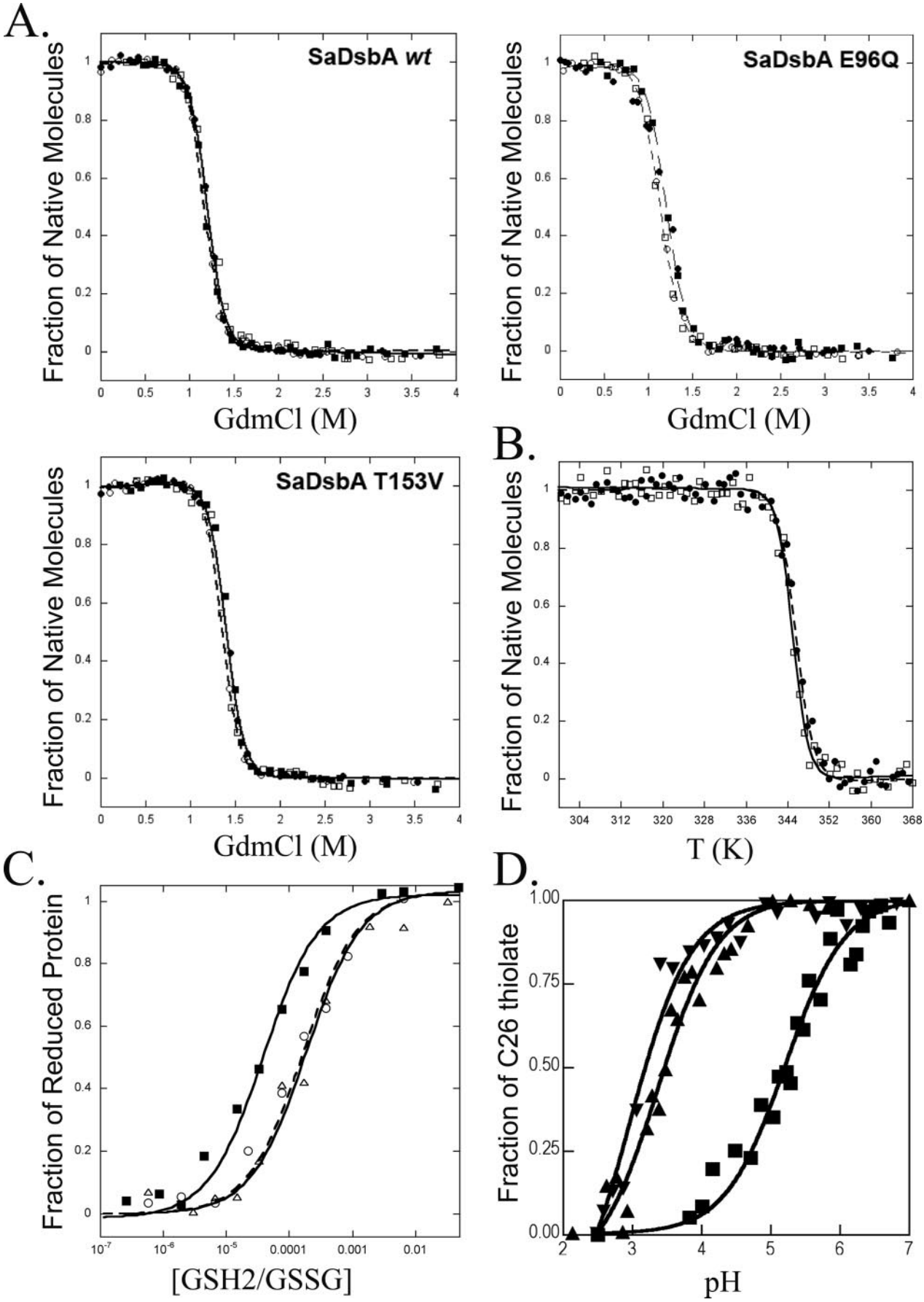

TABLE 2

Free energy of stabilization of oxidized and reduced SaDsbA, SaDsbA variants, and EcDsbA and redox potential and pK_a values for SaDsbA, SaDsbA variants, and EcDsbA

	Redox state	Midpoint of transition	Cooperativity of transition	ΔG_{stab}	$\Delta\Delta G_{ox/red}$	T_m
		M GdmCl	*kJmol^{-1}M^{-1}*	*kJ/mol*	*kJ/mol*	*K*
SaDsbAwt	Oxidized	1.20	25.03 ± 0.9	−30.08 ± 1.1	−0.21 ± 2.8	345.6 ± 0.09
	Reduced	1.17	25.56 ± 1.4	−29.87 ± 1.7		345.1 ± 0.08
SaDsbAT153V	Oxidized	1.42	24.45 ± 1.8	−34.25 ± 2.6	0.97 ± 4.3	344.9 ± 0.16
	Reduced	1.38	26.06 ± 1.2	−35.22 ± 1.7		346.2 ± 0.08
SaDsbA E96Q	Oxidized	1.19	21.38 ± 1.5	−25.64 ± 2.1	−2.8 ± 3.2	347.4 ± 0.09
	Reduced	1.12	20.29 ± 0.9	−22.84 ± 1.1		347.4 ± 0.08
EcDsbAwt	Oxidized	1.66[a]	20.07 ± 0.7[a]	−33.5 ± 1.2[a]	14.8 ± 4.0[a]	342.4 ± 0.52
	Reduced	2.14[a]	22.6 ± 1.3[a]	−48.3 ± 2.8[a]		350.6 ± 0.25

	K_{eq}	Redox potential	pK_a
	M	*mV*	
SaDsbAwt	$2.0 \pm 0.3 \times 10^{-4}$ ($2.09 \pm 0.27 \times 10^{-4}$)[b]	−132 (−131)[b]	3.37 (±0.07)
SaDsbA T153V	$1.6 \pm 0.29 \times 10^{-4}$	−129	5.21 (±0.08)
SaDsbA E96Q	$4.0 \pm 0.5 \times 10^{-5}$	−111	3.09 (±0.08)
EcDsbAwt	$1.2 \pm 0.05 \times 10^{-4}$[a]	−122[a]	3.28 (±0.09)[a]

[a] Ref. 40.
[b] Ref. 26.

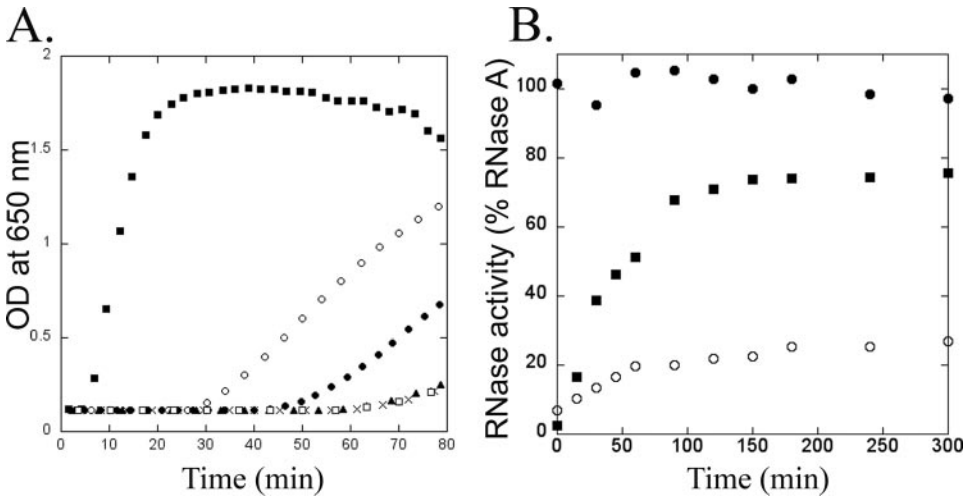

FIGURE 5. *A*, insulin reduction assay. The reaction mixtures contained 131 μM insulin in 0.1 M phosphate buffer, pH 7.0, 2 mM EDTA. The reaction was performed in the absence (*x*) or presence of a disulfide oxidoreductase (5 μM EcDsbC (■), 10 μM EcDsbA (○), 10 μM SaDsbA (▲), 10 μM SaDsbA T153V (●), 10 μM SaDsbA E96Q (□)). Reactions were started by adding DTT to a final concentration of 0.35 mM, and the aggregation of reduced insulin was followed 650 nm every 30 s. *B*, refolding of scrambled RNase. Reshuffling of scRNase was carried out by incubating the scrambled enzyme (40 μM) in 100 mM sodium phosphate, NaOH, pH 7.0, 1 mM EDTA, 10 μM DTT, and in the presence of 10 μM EcDsbC (■) or SaDsbA (○). Folded RNase was used as a positive control (●). The cleavage of cCMP by native RNase A was followed spectroscopically at 296 nm.

notion that this residue is involved in substrate interactions and that Thr and Val residues preceding *cis*-Pro confer different binding characteristics.

Disulfide Isomerase Activity—SaDsbA contains residues characteristic of the disulfide isomerases DsbC and DsbG (D and Y in the D*XXCX*YC motif, Thr in *cis*-Pro loop). To assess whether these residues confer isomerase activity, we determined the SaDsbA catalyzed recovery of active RNase A from oxidized, scrambled RNase A (scRNase) (45). In this assay, the isomerase DsbC yields 80% of active molecules (Fig. 5*B*) whereas SaDsbA has an activity similar to that of the oxidase EcDsbA, with 20% active RNase A after 300 min under the applied conditions (Fig. 5*B*). SaDsbA mutants did not show any activity in this assay.

DISCUSSION

Disulfide bonds between cysteine residues contribute to the stability and activity of many secretory proteins, and organisms contain complex enzymatic systems to promote catalysis of disulfide bond formation. These enzymatic pathways have been extensively studied in *E. coli* (reviewed in Ref. 3, 58). Functional homologues of Dsb proteins have also been found in Gram-positive bacteria (15–22); however our knowledge of the processes of oxidative folding in these organisms is scarce. Moreover, investigations of Gram-positive Dsb proteins indicate that we may not be able to directly extrapolate the mechanisms observed in *E. coli* to these organisms. For example, functional and structural characterization of *M. tuberculosis* DsbE (22) showed that it is an oxidant even though its structure and sequence resemble that of CcmG (DsbE), a Gram-negative disulfide reductant.

FIGURE 4. *A*, GdmCl induced unfolding/refolding equilibria of wild-type SaDsbA and variants at pH 7.0 and 25 °C. The transitions were measured fluorimetrically at 330 nm. *Solid symbols* represent oxidized proteins, and *open symbols* represent reduced proteins. *Circles* correspond to the unfolding transitions and *squares* to the refolding transitions. The normalized fluorescence data for the oxidized (●, ■), and reduced (○, □) protein were fitted to a two-state model of folding (*solid* and *dashed lines*, respectively). *B*, thermal unfolding of wild-type SaDsbA measured in 100 mM sodium phosphate/NaOH, 1 mM EDTA pH 7.0 (reduced SaDsbA was measured in the presence of 0.75 mM DTT). ● and □ represent oxidized and reduced SaDsbA respectively. *C*, redox equilibria of SaDsbA (△), SaDsbA T153V (○), and SaDsbA E96Q (■) with glutathione at pH 7.0 and 25 °C. The fraction of reduced SadsbA was determined using the specific SaDsbA fluorescence at 335 nm (excitation 280 nm) and fitted as previously described (40). *D*, determination of the pK_a of the nucleophilic cysteine (Cys^{26}) in SaDsbA (▲), SaDsbA E96Q (▼), SaDsbA T153V (■). The pH dependence of the thiolate-specific absorbance signal ($S = (A_{240}/A_{280})_{reduced}/(A_{240}/A_{280})_{oxidized}$) was fitted according to the Henderson-Hasselbach equation (the oxidized proteins were used as a reference).

Our work also shows that despite the overall structural similarity, SaDsbA does not operate in the same way as EcDsbA. The structural fold of SaDsbA is typical of DsbA disulfide oxidants from Gram-negative bacteria (Fig. 1*A*). However, it has a truncated binding groove and a charged rather than hydrophobic surface surrounding the redox active site (Figs. 1, *B* and *C* and 3*A*). These structural differences suggest that the two proteins have different substrate specificities. This was confirmed in that EcDsbA catalyzes insulin reduction whereas SaDsbA does not. A single SaDsbA mutation (T153V) in the *cis*-Pro loop (which is known to be involved in substrate binding (50–52)) partially restored activity in this reaction.

Sequence alignment showed that these characteristics of SaDsbA are generally conserved among Gram-positive DsbAs (Fig. 2*A*). Most Gram-positive sequences have a similar deletion at the C-terminal segment compared with EcDsbA, and therefore are also likely to have a truncated groove. Also, Gram-positive DsbAs have acidic residues in the loop connecting helices α3 and α4 that are located close to the active site.

SaDsbA, like EcDsbA, has an oxidizing redox potential (E'_0 −131 mV and −122 mV, respectively) (26, 40). Interestingly, the acidic residue Glu^{96} in the α3-α4 loop adjacent to the active site, decreases the redox potential. When SaDsbA Glu^{96} is mutated to Q, the redox potential increases from −131 mV (26) to −111 mV (Fig. 4*C*). This suggests that Glu^{96} plays an important role in controlling the oxidative strength of SaDsbA.

A major characteristic of EcDsbA that contributes to its highly oxidizing nature is its unstable disulfide bond (56) as well as an unusually low pK_a for the nucleophilic cysteine (42). Surprisingly, we found that the strongly oxidizing redox potential of SaDsbA does not arise from an unstable disulfide. Both chemically and thermally induced unfolding experiments showed that oxidized and reduced SaDsbA have equivalent thermodynamic stabilities (Fig. 4, *A* and *B* and Table 2).

The redox potential of SaDsbA might derive from the low pK_a (3.37) of the nucleophilic cysteine Cys^{26} (Fig. 4*D* and Table 2B), which is similar to that of EcDsbA (3.3 (40)). One factor contributing to the low pK_a for Cys^{30} in EcDsbA, is stabilization of the thiolate by hydrogen bonding to the His side chain in the CH*X*C motif (40, 59). SaDsbA has a Tyr rather than a His, but the catalytic C*XX*C is flanked on either side by basic residues that could help to stabilize a thiolate anion (Fig. 2*B*). However, an acidic residue close to the active site (*e.g.* Glu^{96}), destabilizes the thiolate as has been shown for other redox-active proteins (60). This was broadly borne out, in that replacement of the acidic residue with a polar residue (E96Q), dropped the pK_a of the nucleophylic cysteine even further (pK_a 3.09) and increased the redox potential to −111 mV (Fig. 4*C* and Table 2B). The Thr in the *cis*-Pro loop was found to have a major effect on pK_a in that mutation to Val increased it from 3.37 to 5.21 (Fig. 4*D*). This change to the pK_a may be due to removal of a water-mediated hydrogen bond to the Cys^{26} thiolate in the T153V variant as observed in the crystal structure (Fig. 2*B*).

A major difference between SaDsbA and EcDsbA is that SaDsbA does not require a DsbB for activity (15, 26). Indeed, *S. aureus* does not encode a DsbB (26). In agreement with these findings we showed that the structure of SaDsbA cannot interact with DsbB in the same way that EcDsbA does (Fig. 3*B*) (49), and a direct assay of DsbB activity showed that EcDsbA causes quinone reduction by EcDsbB but SaDsbA does not (Fig. 3*C*). An important implication of these findings is that *S. aureus* uses a very different mechanism to that of *E. coli* for forming disulfides in secreted proteins, relying on the equivalent stabilities of the oxidized and reduced forms so that oxidizing agents such as molecular oxygen in the extracellular milieu may be all that is necessary to convert the reduced form to the functionally active oxidized form.

In conclusion, despite similar folds, oxidizing potentials and nucleophilic cysteine pK_as, SaDsbA from the Gram-positive pathogen *S. aureus* has a different mechanism than EcDsbA to recover its active oxidized form. This mechanism is likely to be based on the similar thermodynamic stabilities of the oxidized and reduced forms of SaDsbA, that could ensure efficient recovery of the oxidized form through extracellular oxidants. SaDsbA thus needs only the presence of oxidizing agents in the extracellular environment to access the catalytically active oxidized form. Moreover, this mechanism could be common to an entire subgroup of Gram-positive organisms that encode a DsbA but not a DsbB, including the important pathogens *E. faecalis* and *L. monocytogenes*.

Acknowledgments—We thank Karl A. Byriel for assistance with data collection at the University of Queensland ROCX Diffraction Facility, Tom Alber and Nat Echols for measuring MAD data at the Advanced Light Source, which is supported by the Director, Office of Science, Office of Basic Energy Sciences, of the U. S. Dept. of Energy under Contract DE-AC02-05CH11231. We thank the Australian Research Council Special Research Centre for the use of their facilities.

REFERENCES

1. Gruber, C. W., Cemazar, M., Heras, B., Martin, J. L., and Craik, D. J. (2006) *Trends Biochem. Sci.* **31,** 455–464
2. Messens, J., and Collet, J. F. (2006) *Int. J. Biochem. Cell Biol.* **38,** 1050–1062
3. Kadokura, H., Katzen, F., and Beckwith, J. (2003) *Annu. Rev. Biochem.* **72,** 111–135
4. Nakamoto, H., and Bardwell, J. C. (2004) *Biochim. Biophys. Acta* **1694,** 111–119
5. Bardwell, J. C. A., Lee, J. O., Jander, G., Martin, N., Belin, D., and Beckwith, J. (1993) *Proc. Natl. Acad. Sci. U. S. A.* **90,** 1038–1042
6. Peek, J. A., and Taylor, R. K. (1992) *Proc. Natl. Acad. Sci. U. S. A.* **89,** 6210–6214
7. Yu, J., and Kroll, J. S. (1999) *Microbes Inf.* **1,** 1221–1228
8. Stenson, T. H., and Weiss, A. A. (2002) *Infect. Immun.* **70,** 2297–2303
9. Ha, U. H., Wang, Y., and Jin, S. (2003) *Infect. Immun.* **71,** 1590–1595
10. Ellermeier, C. D., and Slauch, J. M. (2004) *J. Bacteriol.* **186,** 68–79
11. Okamoto, K., Baba, T., Yamanaka, H., Akashi, N., and Fujii, Y. (1995) *J. Bacteriol.* **177,** 4579–4586
12. Miki, T., Okada, N., and Danbara, H. (2004) *J. Biol. Chem.* **279,** 34631–34642
13. Pooley, H. M., Merchante, R., and Karamata, D. (1996) *Microb. Drug Resist.* **2,** 9–15
14. Matias, V. R., and Beveridge, T. J. (2006) *J. Bacteriol.* **188,** 1011–1021
15. Kouwen, T. R., van der Goot, A., Dorenbos, R., Winter, T., Antelmann, H., Plaisier, M. C., Quax, W. J., van Dijl, J. M., and Dubois, J. Y. (2007) *Mol. Microbiol.* **64,** 984–999
16. Ishihara, T., Tomita, H., Hasegawa, Y., Tsukagoshi, N., Yamagata, H., and Udaka, S. (1995) *J. Bacteriol.* **177,** 745–749
17. Erlendsson, L. S., and Hederstedt, L. (2002) *J. Bacteriol.* **184,** 1423–1429
18. Dorenbos, R., Stein, T., Kabel, J., Bruand, C., Bolhuis, A., Bron, S., Quax, W. J., and Van Dijl, J. M. (2002) *J. Biol. Chem.* **277,** 16682–16688

19. Sarvas, M., Harwood, C. R., Bron, S., and van Dijl, J. M. (2004) *Biochim. Biophys. Acta* **1694,** 311–327
20. Meima, R., Eschevins, C., Fillinger, S., Bolhuis, A., Hamoen, L. W., Dorenbos, R., Quax, W. J., van Dijl, J. M., Provvedi, R., Chen, I., Dubnau, D., and Bron, S. (2002) *J. Biol. Chem.* **277,** 6994–7001
21. Stein, T. (2005) *Mol. Microbiol.* **56,** 845–857
22. Goulding, C. W., Apostol, M. I., Gleiter, S., Parseghian, A., Bardwell, J., Gennaro, M., and Eisenberg, D. (2004) *J. Biol. Chem.* **279,** 3516–3524
23. Hovde, C. J., Marr, J. C., Hoffmann, M. L., Hackett, S. P., Chi, Y. I., Crum, K. K., Stevens, D. L., Stauffacher, C. V., and Bohach, G. A. (1994) *Mol. Microbiol.* **13,** 897–909
24. Dziewanowska, K., Edwards, V. M., Deringer, J. R., Bohach, G. A., and Guerra, D. J. (1996) *Arch. Biochem. Biophys.* **335,** 102–108
25. Krupka, H. I., Segelke, B. W., Ulrich, R. G., Ringhofer, S., Knapp, M., and Rupp, B. (2002) *Protein Sci.* **11,** 642–651
26. Dumoulin, A., Grauschopf, U., Bischoff, M., Thony-Meyer, L., and Berger-Bachi, B. (2005) *Arch. Microbiol.* **184,** 117–128
27. Heras, B., Kurz, M., Jarrott, R., Byriel, K. A., Jones, A., Thöny-Meyer, L., and Martin, J. L. (2007) *Acta Crystallogr. F.* **63,** 953–956
28. Heras, B., Edeling, M. A., Byriel, K. A., Jones, A., Raina, S., and Martin, J. L. (2003) *Structure* **11,** 139–145
29. Otwinowski, Z., and Minor, W. (1997) *Methods Enzymol.* **276,** 307–326
30. Terwilliger, T. C., and Berendzen, J. (1999) *Acta Crystallogr. D. Biol. Crystallogr.* **55,** 849–861
31. Perrakis, A., Morris, R., and Lamzin, V. S. (1999) *Nat. Struct. Biol.* **6,** 458–463
32. Jones, T. A., Zou, J. Y., Cowan, S. W., and Kjeldgaard. (1991) *Acta Crystallogr. A.* **47,** 110–119
33. Emsley, P., and Cowtan, K. (2004) *Acta Crystallogr. D. Biol. Crystallogr.* **60,** 2126–2132
34. Brunger, A. T., Adams, P. D., Clore, G. M., DeLano, W. L., Gros, P., Grosse-Kunstleve, R. W., Jiang, J. S., Kuszewski, J., Nilges, M., Pannu, N. S., Read, R. J., Rice, L. M., Simonson, T., and Warren, G. L. (1998) *Acta Crystallogr. D. Biol. Crystallogr.* **54,** 905–921
35. Storoni, L. C., McCoy, A. J., and Read, R. J. (2004) *Acta Crystallogr. D. Biol. Crystallogr.* **60,** 432–438
36. Kraulis, P. J. (1991) *J. Appl. Crystallogr.* **24,** 946–950
37. DeLano, W. L. (2002) *DeLano Scientific*, San Carlos, CA
38. Nicholls, A., Sharp, K. A., and Honig, B. (1991) *Proteins* **11,** 281–296
39. Santoro, M. M., and Bolen, D. W. (1988) *Biochemistry* **27,** 8063–8068
40. Huber-Wunderlich, M., and Glockshuber, R. (1998) *Fold Des.* **3,** 161–171
41. Mossner, E., Huber-Wunderlich, M., Rietsch, A., Beckwith, J., Glockshuber, R., and Aslund, F. (1999) *J. Biol. Chem.* **274,** 25254–25259
42. Nelson, J. W., and Creighton, T. E. (1994) *Biochemistry* **33,** 5974–5983
43. Holmgren, A. (1979) *J. Biol. Chem.* **254,** 3664–3671
44. Bader, M. W., Xie, T., Yu, C. A., and Bardwell, J. C. (2000) *J. Biol. Chem.* **275,** 26082–26088
45. Hillson, D. A., Lambert, N., and Freedman, R. B. (1984) *Methods Enzymol.* **107,** 281–294
46. Hendrickson, W. A. (1991) *Science* **254,** 51–58
47. Hendrickson, W. A., Horton, J. R., and LeMaster, D. M. (1990) *EMBO J.* **9,** 1665–1672
48. Martin, J. L., Bardwell, J. C. A., and Kuriyan, J. (1993) *Nature* **365,** 464–468
49. Inaba, K., Murakami, S., Suzuki, M., Nakagawa, A., Yamashita, E., Okada, K., and Ito, K. (2006) *Cell* **127,** 789–801
50. Qin, J., Clore, G. M., Kennedy, W. P., Kuszewski, J., and Gronenborn, A. M. (1996) *Structure* **4,** 613–620
51. Kadokura, H., Tian, H. P., Zander, T., Bardwell, J. C. A., and Beckwith, J. (2004) *Science* **303,** 534–537
52. Charbonnier, J. B., Belin, P., Moutiez, M., Stura, E. A., and Quemeneur, E. (1999) *Protein Sci.* **8,** 96–105
53. Hiniker, A., Ren, G., Heras, B., Zheng, Y., Laurinec, S., Jobson, R. W., Stuckey, J. A., Martin, J. L., and Bardwell, J. C. (2007) *Proc. Natl. Acad. Sci. U. S. A.* **104,** 11670–11675
54. Guddat, L. W., Bardwell, J. C. A., Zander, T., and Martin, J. L. (1997) *Protein Sci.* **6,** 1148–1156
55. Zapun, A., Bardwell, J. C., and Creighton, T. E. (1993) *Biochemistry* **32,** 5083–5092
56. Wunderlich, M., and Glockshuber, R. (1993) *Protein Sci.* **2,** 717–726
57. Pace, C. N. (1986) *Methods Enzymol.* **131,** 266–280
58. Masip, L., Pan, J. L., Haldar, S., Penner-Hahn, J. E., DeLisa, M. P., Georgiou, G., Bardwell, J. C., and Collet, J. F. (2004) *Science* **303,** 1185–1189
59. Guddat, L. W., Bardwell, J. C. A., Glockshuber, R., HuberWunderlich, M., Zander, T., and Martin, J. L. (1997) *Protein Sci.* **6,** 1893–1900
60. Lewin, A., Crow, A., Oubrie, A., and Le Brun, N. E. (2006) *J. Biol. Chem.* **281,** 35467–35477

Figure S1. Close up view of the SaDsbA (left) and EcDsbA (right) active sites showing the catalytic cysteines (^{26}CXYC^{29} SaDsbA and ^{30}CXHC^{33} EcDsbA) and the residues in the *cis*-proline loop (^{153}T-*cis*P^{154} SaDsbA and ^{150}V-*cis*P^{151} EcDsbA). The residues that map to the hydrophobic patch adjacent to the active site in EcDsbA (including F29, ^{63}FMGG^{66}, L68, V96) are mostly replaced or covered with charged residues in SaDsbA (K25, ^{59}FLGK^{62}, D63, K98-E99). Additionally, the different position of the α3–α4 loop in SaDsbA also places the negative residue E96 in the proximity of the active site.

Figure 1S

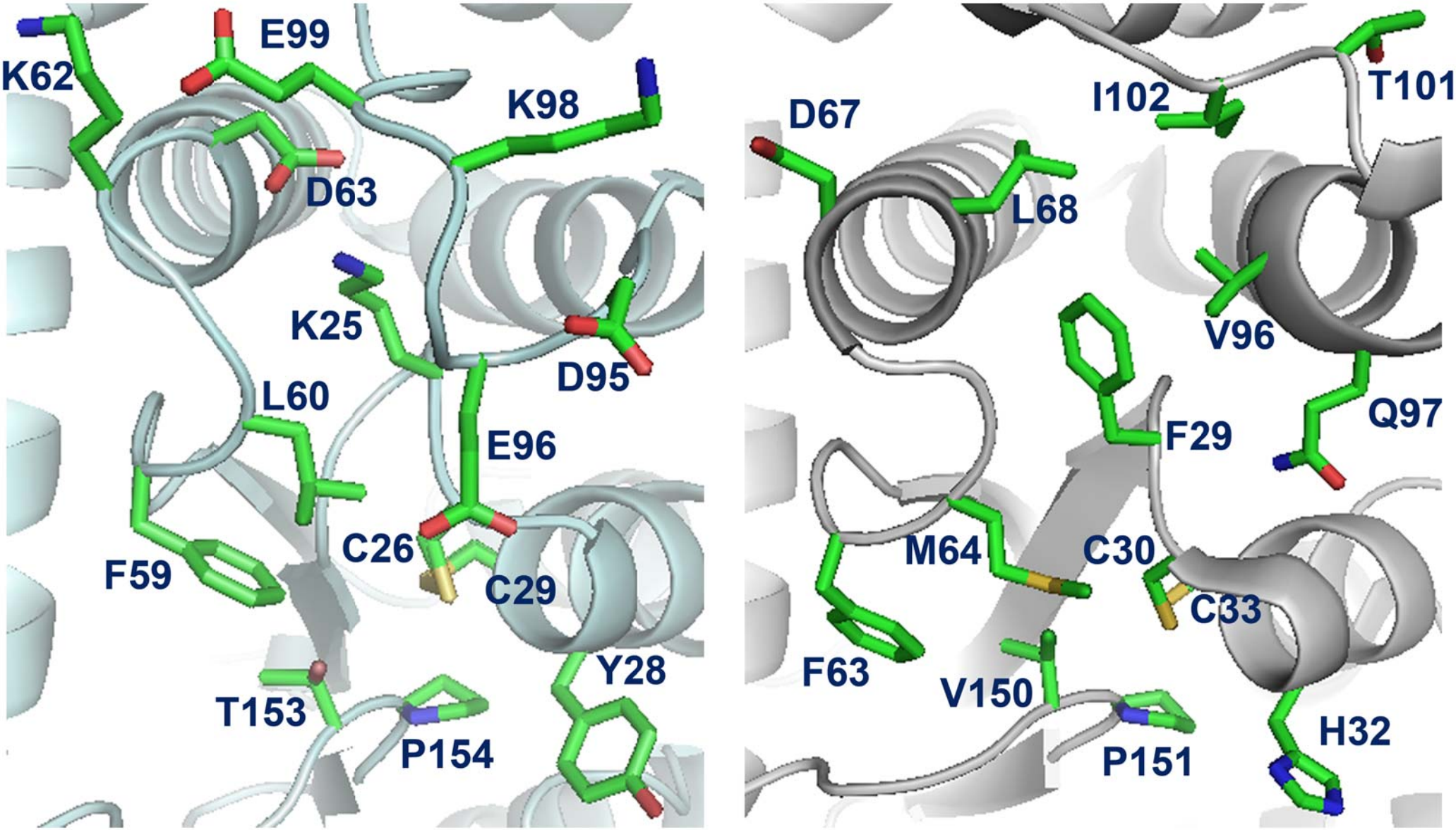
K62
E99
K98
D63
K25
D95
L60
E96
C26
C29
F59
Y28
T153
P154
D67
I102
T101
L68
V96
Q97
F29
M64
C30
C33
F63
V150
H32
P151

Staphylococcus aureus DsbA Does Not Have a Destabilizing Disulfide: A NEW PARADIGM FOR BACTERIAL OXIDATIVE FOLDING

Begoña Heras, Mareike Kurz, Russell Jarrott, Stephen R. Shouldice, Patrick Frei, Gautier Robin, Masa Cemazar, Linda Thöny-Meyer, Rudi Glockshuber and Jennifer L. Martin

J. Biol. Chem. 2008, 283:4261-4271.
doi: 10.1074/jbc.M707838200 originally published online December 12, 2007
